Tracking the Transformation of Nanoparticulate and Ionic Silver at Environmentally Relevant Concentration Levels by Hollow Fiber Flow Field-Flow Fractionation Coupled to ICPMS

Zhi-Qiang Tan,[†] Yong-Guang Yin,[†] Xiao-Ru Guo,[†] Meseret Amde,[†] Myeong Hee Moon,[‡] Jing-Fu Liu,*[,†] and Gui-Bin Jiang[†]

[†]State Key Laboratory of Environmental Chemistry and Ecotoxicology, Research Center for Eco-Environmental Sciences, Chinese Academy of Sciences, Beijing 100085, China

[‡]Department of Chemistry, Yonsei University, Seoul 03722, Korea

Ⓢ Supporting Information

ABSTRACT: It is a great challenge to monitor the physical and chemical transformation of nanoparticles at environmentally relevant concentration levels, mainly because the commonly used techniques like dynamic light scattering and transmission electron microscopy are unable to characterize and quantify trace level nanoparticles in complex matrices. Herein, we demonstrate the on-line coupled system of hollow fiber flow field-flow fractionation (HF5), minicolumn concentration, and inductively coupled plasma mass spectrometry (ICPMS) detection as an efficient approach to study the aggregation and chemical transformation of silver nanoparticles (AgNPs) and ionic Ag species in the aqueous environment at ng/mL levels. Taking advantage of the in-line dialysis of HF5, the selective capture of Ag(I) species by the resin in minicolumn, and the high selectivity and sensitivity of ICPMS detection, we recorded the aggregation of 10 ng/mL AgNPs in complex matrices (e.g., NOM, Na$^+$/Ca^{2+}), revealing an interesting tiny AgNPs formation process of photoreduction of trace level Ag(I) that is different from larger AgNPs generated at high concentration of Ag(I) by accurate characterization and respectively identifying and quantifying new thiol-complexed Ag(I) and residual Ag(I) in the intertransformation of Ag(I) and AgNPs in domestic wastewater by simultaneously detecting the S and Ag signals via ICPMS.
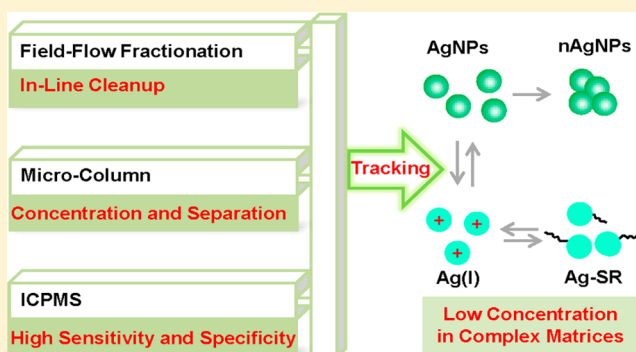
INTRODUCTION

Silver nanoparticles (AgNPs) have drawn remarkable attention from the scientific community in recent years, mainly due to their wide applications, high environmental reactivity, and potential risks.[1−3] Once released into aquatic environments, AgNPs are likely to undergo a variety of transformations like aggregation,[4−6] dissolution, and rereduction,[7,8] which can affect the transport, bioavailability, and toxicity of AgNPs.

To understand the transformations and potential risk of AgNPs, it is crucial to characterize and determine the pristine AgNPs and formed Ag species at environmentally relevant conditions. Studying the aggregation processes of AgNPs is of importance as it significantly affects its transport, transformation, and toxicity in the environment.[7] However, evaluating the aggregation of AgNPs at environmentally relevant concentrations in complex matrices remains challenging. While dynamic light scattering (DLS) serves as a classic technique to monitor the size change in studying the aggregation of AgNPs,[9] it is unable to distinguish AgNPs from the coexisting suspended particulates such as natural organic matter (NOM) aggregates with nano- to micrometer

size. More importantly, the low sensitivity of DLS makes it only applicable for measuring particulate materials at relatively high concentration (e.g., μg/mL).[10−12] Transmission electron microscopy (TEM) is also usually used to probe the size distribution and variation of AgNPs, but either TEM observation has to be performed at relatively high nanoparticle concentrations (>μg/mL) or a lot of TEM images are needed to obtain their particle size information.[13]

Besides aggregation, it is also important to understand the chemical transformation of AgNPs and ionic Ag species (IAg) that is relevant to the size- and species-correlated toxicological effects in the environment. Because of the medium redox potential of silver,[14] both oxidative dissolution of AgNPs into Ag(I) and reduction of Ag(I) into AgNPs were observed simultaneously in the environment,[15−18] thus IAg and AgNPs are deemed to be coexisting in AgNPs colloids and the

environment. Moreover, it was generally recognized that IAg and small-sized AgNPs express a pronounced toxic effect in comparison to that of the large-sized AgNPs.[19−21] Therefore, it is essential to distinguish the various environmentally relevant chemical species of AgNPs. Ultrafiltration[22] or cloud point extraction[23] could effectively achieve separation of IAg from AgNPs but commonly were used as off-line pretreatments before characterization or quantification. Although X-ray absorption fine structure or X-ray fluorescence spectroscopies showed excellent separation resolution for Ag species in complex matrices,[24,25] these techniques failed to directly analyze Ag species at environmentally relevant concentration levels due to their limited sensitivity. Inductively coupled plasma-mass spectrometry (ICPMS) featured with accurate determination of elements and multielemental analysis with high sensitivity and wide dynamic range.[26] Single-particle ICPMS (SP-ICPMS) has gained great attention in analysis of AgNPs and dissolved Ag(I) with the advantage of simplicity and speed, but its applicability in complex samples is limited due to matrix effects.[27,28] Moreover, the size characterization sensitivity is low (∼20 nm) for AgNPs.[29] Therefore, coupling efficient and robust separation techniques with sensitive detectors (e.g., ICPMS) would pave an effective way for accurate quantification and tracking transformation of Ag species at environmentally relevant concentration levels in the environment.

Among hyphenated techniques with ICPMS as the detector, field-flow fractionation (FFF) served as competitive choice to characterize AgNPs due to the mild separation, high selectivity, and broad application in continuous size separation range (e.g., 1 nm to 100 μm).[30−32] Among the FFF techniques, flow FFF was considered as the most universal mainly due to its simplicity in instrument and operation and versatility in various targets analysis; thus, flow FFF coupled with ICPMS was regarded as one of the most promising tools to characterize AgNPs.[33−35] Poda et al. employed flow FFF coupled with ICPMS to investigate particle size distribution of AgNPs in aqueous matrices including biological matrices after exposure and obtained comparable size results with that of DLS and TEM.[36] Recently, Lee et al. described the potential applicability of flow FFF off-line hyphenated with SP-ICPMS in characterizing AgNPs in real aqueous samples.[37] Collectively, the hyphenation of AF4 and ICP-MS proved to be a suitable technique for AgNPs separation and characterization in various matrices. However, in the focusing step in flow FFF, Ag(I) and tiny AgNPs with diameter less than the membrane pore were dialyzed and discarded as waste;[35,36] thus, there is no published study focused on speciation analysis of IAg and AgNPs using conventional flow FFF based methods. Hollow fiber flow field-flow fractionation (HF5), as an emerging variant of flow FFF, features low cost in disposable channels and simple assembly, which effectively reduced the run-to-run sample carryover problem from the sample matrix.[38] In HF5, separation was conducted in a cylindrical HF membrane instead of the thin ribbon-like open channel in conventional flow FFF, and the flow field was applied perpendicularly to the HF axial direction. Compared with the AF4 channel, the low channel volume of HF5 channel resulted in less sample dilution. The reduced radial flow rate used in HF5 made it more compatible with various detectors (especially ICPMS), and sample fractions dialyzed during focusing process and eluted during fractionation process could be easily collected for further analysis.[39] A recent study described the coupling of HF5 with multi angle

light scattering detector to characterize the dispersed AgNPs in aqueous media and to quantify off-line the separately collected Ag(I) and AgNPs.[40] To improve applicability of HF5-based method in Ag speciation analysis, we recently on-line coupled HF5 and minicolumn concentration (MCC) with multiple detectors including UV−vis spectrometer (UV), DLS, and ICPMS for identification, characterization, and quantification of two IAg(I) species and five differently sized AgNPs at ng/mL level,[41] demonstrating its potential for studying the transformation of Ag species at environmentally relevant concentrations.

In this work, by using our recently developed hyphenated method,[41] we investigated the aggregation and chemical transformation of AgNPs and IAg species in aqueous environments at environmentally relevant concentrations. The aggregation of trace levels of AgNPs in the presence of NOM and Na$^+$/Ca^{2+} was monitored for the first time via the size distribution and variation of AgNPs depicted in the ICPMS elution profiles. The chemical transformation products of Ag(I), differently sized AgNPs, and thiol-complexed Ag(I) were also identified and quantified in sun-lit NOM-solutions and domestic wastewaters, respectively.

■ MATERIALS AND METHODS

Chemicals and Materials. Citrate-coated AgNPs with nominal sizes of 10 nm (10 nm AgNP) and 20 nm (20 nm AgNP) (each 20 μg/mL) were bought from Sigma-Aldrich (St. Louis, MO). Ag(I) standard solution (GSB04−1712−2004) at concentration of 1000 μg/mL was purchased from the National Institute of Metrology (Beijing, China). Analytical-grade AgNO$_3$ was obtained from Beijing Chemical Co., Ltd. Suwannee River natural organic matter (SRNOM) (1R101N) was bought from the International Humic Substance Society (St. Paul, MN). L-Cysteine (Cys) (99%) was obtained from J & K Scientific Ltd. (Beijing, China). Surfactant FL-70 and NaN$_3$, two carrier solution additives, were from Thermo (Fair Lawn, NJ) and Ameresco (Framingham, MA), respectively. Gold nanoparticles (Au NPs) with certified diameters of 10 nm (8011), 30 nm (8012), and 60 nm (8013) were purchased from the National Institute of Standards and Technology (NIST, Gaithersburg, MD) and used to calculate AgNPs diameters based on retention time (t_R). Amberlite IR120 resin in sodium, NaClO$_4$, Ca(ClO$_4$)$_2$, Na$_2$S$_2$O$_3$, and H$_2$O$_2$ were purchased from Sinopharm Chemical Reagent Co. Ltd. (Beijing, China). The resin needed to be cleaned and activated prior to use.[41] Poly(ethersulfone) (PES) HF with a nominal molecular mass cutoff (MWCO) of 10 kDa was bought from Kaihong Membrane Technology Co., Inc. (Hangzhou, China).

Characterization and Quantification of Various Ag Species. HF5 was on-line coupled with MCC and dual detectors including UV and ICPMS (HF5/MCC-UV/ICPMS) to achieve the separation, characterization, and quantification of various Ag species. Detailed configuration and operation of the hyphenated system are described elsewhere[41] and also provided in the Supporting Information. Briefly, the whole analytical run cycle consist of three on-line steps: (I) focusing/relaxation of AgNPs and isolation of Ag(I) species, (II) fractionation, characterization, and quantification of AgNPs, and (III) quantification of Ag(I) species. Given that particle retention in HF5 is dependent on the size, the particle size or size distribution of the target particles can be calculated with standard particles (e.g., AuNPs).[40,42] Considering the material-dependent retention behavior possibly due to the particle−
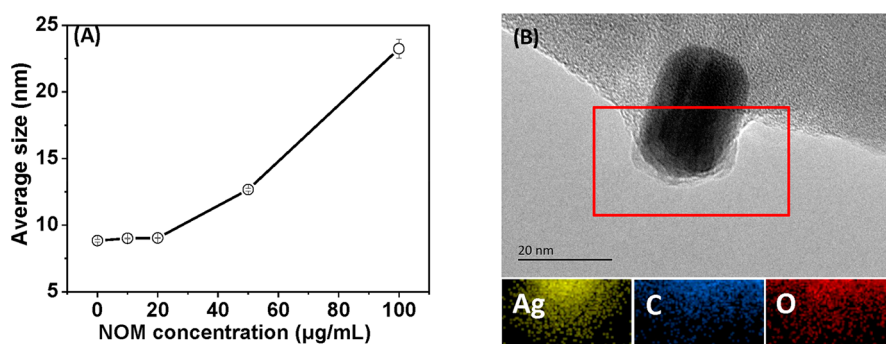
Figure 1. Effect of the NOM concentration on the average size of AgNPs (10 nm AgNP, 10 ng/mL) in the presence of different amount of NOM (0, 10, 20, 50, and 100 μg/mL DOC) (A) and STEM images and EDS mapping results of Ag, C and O (5 μg/mL 10 nm AgNPs in 50 μg/mL NOM).

particle and particle−accumulation-wall interactions,[43] in step II the AgNPs size was obtained with a calibration curve obtained by plotting t_R measured under the same fractionation conditions against the known size of standard AuNPs (Figure S2A), the acceptable standard metallic NPs,[44] from ICPMS fractograms of the Au (^{197}Au) and Ag (^{107}Ag) signals (Figure S2B), and concentrations of fractioned AgNPs were acquired by ICPMS (7700 series, Agilent Technologies, Palo Alto, CA). Free Ag(I), newly formed Ag(I) complex, and AgNPs with diameter less than the HF pore size, namely, tiny AgNPs, could be quantified respectively as follows: Free Ag(I) ions or weak Ag(I) complexes adsorbed onto the Amberlite IR120 resin through ion-exchange with Na^+ in minicolumn concentration (MCC) during step I were desorbed by $Na_2S_2O_3$ and quantified by ICPMS detector in step III. For tiny AgNPs against absorption by the resin in MCC due to the electrostatic repulsion, they were transferred directly to the detectors and quantified by ICPMS in step I. Strong Ag(I) complexes coeluted with tiny AgNPs in step I could be calculated based on the difference of the detected Ag amount in the step III of the two runs with or without introducing of diluted H_2O_2, respectively. The introducing of diluted H_2O_2 could dissolve tiny AgNPs into Ag^+ and adsorbed onto the Amberlite IR120 resin. Additionally, the HF channel was replaced once the recovery of total Ag (including AgNPs and IAg(I)) in the whole run was less than 65%.

Aggregation of AgNPs in the Presence of NOM and Mono- and Divalent Cations. In view of chloride (e.g., from NaCl, $CaCl_2$) being able to induce the bridging between individual citrate-coated AgNPs due to AgCl deposit from dissolved Ag(I) ions,[45] a series of aqueous solutions of $NaClO_4$ and $Ca(ClO_4)_2$ were chosen to evaluate the influences of mono- and divalent cations on the aggregation of AgNPs (10 ng/mL) in NOM solutions. First, the influences of focusing time and NOM concentration on the size of AgNP aggregates were investigated to confirm the capability of HF5 to maintain AgNPs intact in complex matrices through the whole separation. Furthermore, the scanning transmission electron microscopy (STEM, JEOL, JEM-2010F, Japan) with energy-dispersive X-ray spectroscopy (EDS) is used to determine the shape and the distribution of different elements on the surface of AgNPs incubated with NOM with resolution 0.02 nm at 200 kV. Given that critical coagulation concentrations for 2 μg/mL citrate-coated AgNPs in $NaClO_4$ and $Ca(ClO_4)_2$ were 81.55 and 2.11 mM in the presence of pristine NOM,[9] various amounts of $NaClO_4$ (0.01−100 mM) and $Ca(ClO_4)_2$ (0.001−5 mM) were selected to incubate with 10 ng/mL 10 nm AgNP in

NOM (20 μg/mL dissolved organic matter, DOC) aqueous solution at pH 7.4 (adjusted by 5 mM borate buffer) at room temperature for 1 h. The HF5/MCC-UV/ICPMS system directly provided size information about the AgNPs reacted.

Transformation of Ag(I) into AgNPs under Simulated Natural Conditions. Two significantly different concentrations of $AgNO_3$ (33.97 μg/mL and 33.97 ng/mL, respectively) and SRNOM (20 μg/mL DOC) were separately added into borate buffer (5 mM, pH 8.0) under sunlight. A UV−vis spectrometer (UV-3600, Shimadzu, Japan) was employed to monitor AgNPs generated during the first 6 h. The size of AgNPs formed in 0.2 mM $AgNO_3$ solution was characterized ex situ by high-resolution TEM (2100F, JEOL, Japan; details for TEM sample preparation are described elsewhere).[41] Both a fraction (10-fold dilution) of AgNPs formed in 33.97 μg/mL $AgNO_3$ solution and AgNPs generated in 33.97 ng/mL $AgNO_3$ solution were characterized and directly quantified by our proposed system.

Intertransformation of Ag(I) and AgNPs in Domestic Wastewater. Intertransformation of Ag(I) and AgNPs was conducted in domestic wastewater obtained from a municipal wastewater treatment plant (WWTP) located in Qinghe (Beijing, China). In the preliminary experiment, the concentrations of Ag(I) and AgNPs in the influent of WWTP were found to be below the limit of detection (LOD) of the proposed system. Therefore, the influent was spiked with Ag(I) and 10 nm AgNPs (each 10 ng/mL) for this study. After 1 h, the mixture was directly analyzed by HF5/MCC-DLS/UV/ICPMS system to examine the intertransformation products.

■ RESULTS AND DISCUSSION

Aggregation of AgNPs in the Presence of NOM and Mono- or Divalent Cations. To verify the applicability of the developed HF5/MCC-UV/ICPMS system to characterize the aggregation of AgNPs, the possible impact of the relaxation/focusing step on the size of aggregated AgNPs was assessed by measuring the average size of aggregated AgNPs in NOM (20 μg/mL DOC, average concentration in natural surface water)[46] solutions containing 10 mM $NaClO_4$ and 0.5 mM $Ca(ClO_4)_2$, respectively, with focusing times in the range of 4−8 min. Results presented a slight impact of the focusing time on AgNP aggregation (data not shown). To evaluate in-line cleanup of complex matrices, we compared the t_R values of AgNPs in samples containing just different concentrations of NOM (0, 10, 20, 50, and 100 μg/mL DOC). Interestingly, the elution profile of the ICPMS detector shows a slight gradual increase of t_R from 11.9 ± 0.14 to 17.3 ± 0.26 min (mean ± SD, n = 3) as
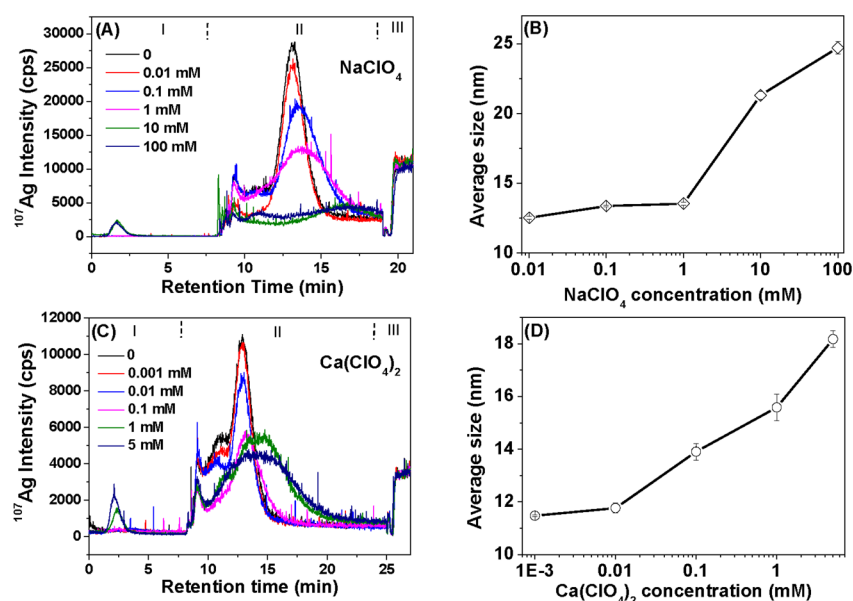
Figure 2. Elution profiles of ICPMS (A and C) and size (B and D) of AgNPs (10 ng/mL 10 nm AgNP) in NOM solution (20 μg/mL DOC). Error bars in B and D represent one standard deviation of three replicates. Operation procedures: focusing/relaxation of AgNPs and isolation of Ag(I) (I), fractionation and characterization of AgNPs (II), and quantification of Ag(I) (III). Experimental conditions: PES HF channel, 10 kDa pore cutoff; injected volume, 100 μL; carrier solution, 0.1% (v/v) FL-70 with 0.02% (w/v) NaN$_3$; inlet flow rate, 1.50 mL/min; radial flow rate, 0.60 mL/min; axial flow, 0.90 mL/min; focusing time, 8 min; eluting flow rate, 0.90 mL/min.

NOM concentration increased from 0 to 100 μg/mL DOC. As shown in Figure 1A, the diameter of the dominant AgNPs, calibrated from the linear regression equation of diameter of the standard AuNPs against t_R, increased from 8.8 ± 0.39 to 23.2 ± 0.70 nm (mean ± SD, n = 3), demonstrating the probable formation of "NOM corona" structures around AgNPs.[47] To testify whether the increase of retention time in the presence of NOM resulted from the carry-over of HF used in complex matrices, we evaluated the AgNPs size variation at a relatively high NOM concentration (50 μg/mL DOC) with a new HF membrane. No significant change in retention times was observed for AgNP colloids injected before and after NOM injection, verifying the fact that the adsorption of NOM onto the membrane was largely minimized due to the electrostatic repulsion in view of the alkaline mobile phase used (pH 9.6) and the negatively charged PES membrane.[48] The identical extended retention time of AgNPs to that by HF used for several times indicates that the changes in t_R (especially in high NOM concentration) could be ascribed to "NOM corona" structures forming rather than the carry-over effect. To further verify the corona structure, STEM-EDS was adopted to investigate nanostructures and element distribution of AgNPs in the NOM solution (50 μg/mL DOC) after incubation at room temperature for 1 h. The red rectangular frame in Figure 1B defines the region for mapping Ag, C, and O distribution. Both C and O enrichment areas significantly overlap Ag-enriched area, demonstrating the NOM wrapping around AgNPs to form corona structure, which could lead to the increment of hydrodynamic size of AgNPs in aqueous solution.

Then, aggregation of 10 ng/mL AgNPs in 20 μg/mL NOM solutions containing various amount of NaClO$_4$ (0.01−100 mM) was studied. Only NOM peaks were found in the initial 8 min of the UV−vis elution profile (Figure S3A), due to the low sensitivity of UV detector. In the HF5-ICPMS elution profile (Figure 2A), both the t_R and peak shape of AgNPs changed with the increase of NaClO$_4$ concentration, demonstrating the

aggregation of AgNPs even in the presence of NOM. The diameter of the dominant AgNPs, calculated from the t_R, progressively increased from 12.5 to 24.7 nm with NaClO$_4$ concentration (0.01−100 mM) (Figure 2B). The aggregation of AgNPs was further investigated in the presence of 0.001−5 mM Ca(ClO$_4$)$_2$. Similar to that of NaClO$_4$, no significant peak of AgNPs was found here in the UV−vis elution profile (Figure S3B). As shown in the ICPMS elution profiles (Figure 2C,D), the dominant AgNP diameter increased from 11.5 to 18.2 nm. Variation in both the retention time and peak shape of the dominant AgNPs eluted in Ca(ClO$_4$)$_2$ solutions was more significant than that in the presence of the same concentration of NaClO$_4$, agreeing with the previous results that Ca^{2+} ions had a greater electrostatic screening effect on AgNPs compared with Na$^+$ ions.[49] Given that the AgNPs colloids used inevitably contain smaller particles with diameters less than the nominate 10 nm, the peak appeared before 10 min in step (II) (Figure 2A,C) may stem from small single dispersed AgNPs.[50] In view of the fact that high ionic strength promotes NOM aggregation,[51] one possible explanation for the slight change of t_R for NOM peaks with increasing salt concentration (Figure S3) is that the compact structure of aggregated NOM at high salt concentrations promotes their dialyzing during focusing. Moreover, the increased ionic strength could effectively shield the electrostatic repulsion between NOM and membrane.[52] Therefore, the retention time of NOM peak decreased with increasing salt concentration. To some extent, NOM could provide charge or steric stabilization of nanomaterial to enhance their dispersion, but this dispersing effect was significantly minimized at higher ionic strength solution.[47] Flow field-flow fractionation, as a mild separation method, has proved to be a successful alternative for DLS in investigating aggregation behavior of nanoparticles,[53,54] but the hyphenation with relatively insensitive detectors (UV or multiangle light scattering) has been an obstacle for its application in low concentration of nanoparticles. In spite of the aggregation of
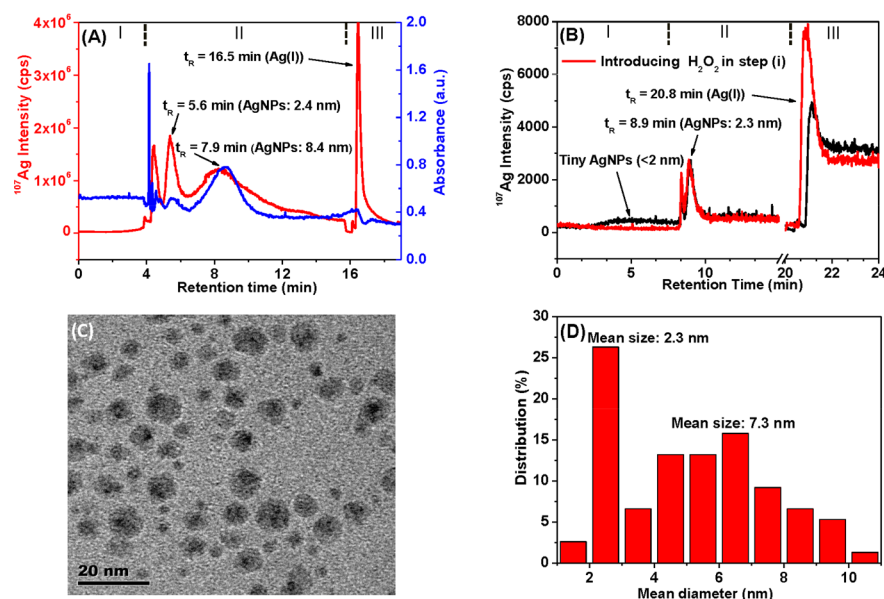
Figure 3. HF5/MCC-UV/ICPMS elution profile of mixtures of NOM and AgNO$_3$ at a concentration of 33.97 μg/mL (A) and 33.97 ng/mL (B), TEM image (C), and size-distribution (D) of the photoreduced AgNPs in NOM solution containing 33.97 μg/mL AgNO$_3$. Operation procedures: focusing/relaxation of AgNPs and isolation of Ag(I) (I), fractionation and characterization of AgNPs (II), and quantification of Ag(I) (III). Experimental conditions: PES HF channel, 10 kDa pore cutoff; injected volume, 100 μL; carrier solution, 0.1% (v/v) FL-70 with 0.02% (w/v) NaN$_3$; inlet flow rate, 1.50 mL/min; radial flow rate, 0.60 mL/min; axial flow, 0.90 mL/min; focusing time, 4 min (A) or 8 min (B); eluting flow rate, 0.90 mL/min.

AgNPs at μg/mL level being similar to that at ng/mL as reported,[9] the hyphenated system here for the first time provided a promising approach to track aggregation of AgNPs at environmentally relevant concentration due to the high-efficiency separation capability of HF5 and sensitive detection of Ag by ICPMS.

Transformation of Ag(I) to AgNPs in Photoreduction of NOM. To compare characterization capability of the proposed method with the TEM method, a high amount of AgNPs was generated in the NOM solution (20 μg/mL DOC) containing 33.97 μg/mL AgNO$_3$ incubated under natural sunlight. The picture (Figure S4A) and the UV−vis spectra (Figure S4B) indicate that the phototransformation of Ag(I) into AgNPs reached equilibrium in less than 6 h. Figure 3A presents the HF5/MCC-UV/ICPMS elution profile of AgNPs and Ag(I) in the irradiated solution after 10-fold dilution, as recorded by UV and ICPMS detectors. The mean particle diameters corresponding to these two peaks (t_R = 5.6 and 7.9 min), calculated from t_R, were around 2.4 and 8.4 nm, agreeing well with the bimodal size distribution (2.3 and 7.3 nm diameter) observed by TEM measurements (Figure 3C,D). It is understandable that the particle diameter measured by TEM is smaller than the hydrodynamic diameter measured by the HF5/MCC-UV/ICPMS (e.g., 7.3 nm by TEM vs 8.4 nm by HF5-ICPMS). For the smaller AgNPs, the similar diameter from TEM (2.3 nm) compared with that from HF5-ICPMS (2.4 nm) again verified the comparable characterization capability of the proposed method with TEM. Therefore, considering the difficulties of TEM in recognizing and counting smaller or tiny AgNPs, the present method could provide more accurate information on a wider range of particle size distributions. The final sharp peak (t_R = 16.5 min) in the ICPMS profile suggests that there was still a large amount of unreacted free Ag(I) in the sample. The relative amount of Ag(I) calculated from the ratio of Ag(I) (t_R = 16.5 min) and

AgNPs (t_R = 5.6 and 7.9 min) is 17.6%, which is slightly lower than the one obtained by ultrafiltration-ICPMS (21%) (details in the Supporting Information). It should be noted that in the ultrafiltration procedure, the photoproduced tiny AgNPs could possibly penetrate the membrane into the filtrate[18] and thus cause an overestimation of the unreacted Ag(I).

A trace amount of AgNO$_3$ as low as 33.97 ng/mL was then reacted with NOM (20 μg/mL DOC) to track the transformation of Ag(I) at environmentally relevant concentrations. As show in Figure 3B, in the focusing/relaxation step (step I, t_R < 8 min), the detected wide peak was ascribed to tiny AgNPs. Two peaks (t_R = 8.4 and 8.9 min) in the fractionation step (step II, 8 min < t_R < 20 min) were assigned to the void peak and larger AgNPs (mean diameter 2.3 nm), respectively. The peak from the residual free or weak complex of Ag(I) trapped by the resin and desorbed by Na$_2$S$_2$O$_3$ was recorded in the elution step (step III, t_R > 20 min). To further verify the assignation of the wide peak (t_R < 8 min), we conducted a second run by introducing diluted H$_2$O$_2$ (2%, v/v) in the radial outlet, in which only tiny AgNPs rather than thiol-binding Ag(I) could be oxidized into Ag(I) as previously observed.[41] This peak disappeared in the second run, and the Ag(I) peak increased correspondingly. The ratio of peak area of tiny AgNPs (t_R < 8 min) in the first run to the incremental peak area of Ag(I) in the second run is 95%, further verifying the wide peak in the focusing/relaxation step almost solely belongs to the tiny AgNPs. The formation of tiny AgNPs and absence of larger AgNPs (e.g., 8.4 nm in Figure 3A) at 21.6 ng/mL Ag(I) precursor suggested that a low concentration of Ag cluster could constrain their fusion and subsequent formation of larger AgNPs.[55] This result also highlights the necessity of studying the transformation of Ag(I) at environmentally relevant concentrations.

It is noteworthy that during the 6 h of irradiation, there is no significant color change for the two NOM solutions with and

without AgNO$_3$ (Figure S4C), which was consistent with the UV−vis results in Figure S4D. Unfortunately, the amount of AgNPs formed were also too low to be identified by TEM, even with more than 50 μL of the AgNPs solution successively loaded on the carbon-coated copper grid (TEM images not shown). These results demonstrated that the proposed method is superior to UV−vis and TEM in tracking tiny AgNPs formation process of photoreduction of trace level Ag(I), which is significantly meaningful considering the low concentration of Ag(I) in real aqueous environments. This study does not aim to simulate real-world formation of AgNPs; instead, it is a fundamental study on understanding the role of NOM in transformation of different amount of Ag(I) to AgNPs. Thus, nucleation and formation of AgNPs with increased incubation time are beyond the scope of the study.

Intertransformation of Ag(I) and AgNPs in Domestic Wastewater. The notable performance of the proposed method encouraged us to further apply it to track the intertransformation of Ag(I) and AgNPs in the influent of WWTP, which is one of the major sinks of the released Ag(I) and AgNPs from industrial and consumer products.[56] As shown in Figure 4, a new peak (t_R = 2.3 min) appeared in the
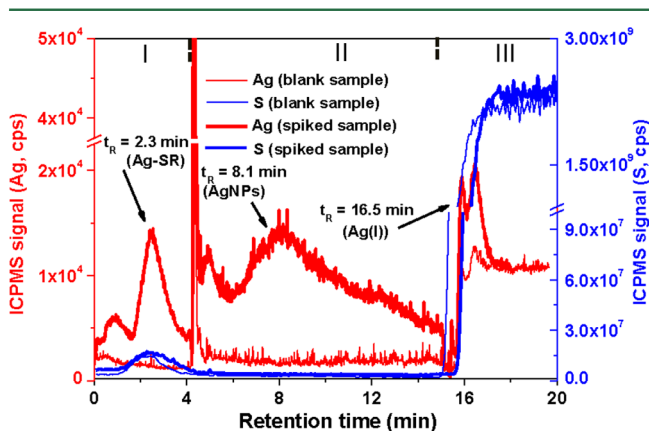

Figure 4. Transformation of AgNPs and Ag(I) (both were spiked at 10 ng/mL) in an influent of WWTP. Operation procedures: focusing/relaxation of AgNPs and isolation of Ag(I) (I), fractionation and characterization of AgNPs (II), and quantification of Ag(I) (III). Experimental conditions: PES HF channel, 10 kDa pore cutoff; injected volume, 100 μL; carrier solution, 0.1% (v/v) FL-70 with 0.02% (w/v) NaN$_3$; inlet flow rate, 1.50 mL/min; radial flow rate, 0.60 mL/min; axial flow, 0.90 mL/min; focusing time, 4 min; eluting flow rate, 0.90 mL/min.

focusing/relaxation step (step I), indicating the spiked Ag(I) and AgNPs (each 10 ng/mL) partially transformed into the thiol-binding Ag(I) (Ag-SR) or tiny AgNPs, though the free Ag(I) can still be detected in the final elution step (step III). In preliminary experiments, the concentration of S^{2-} in the influent sample was found to be less than 2.0 ng/mL, the LOD of ion chromatographic system (ICS-5000, Thermo Fisher Scientific Inc.) equipped for amperometry with a silver working electrode; thus, the transformation of Ag(I) into Ag$_2$S NPs was negligible. To ascertain Ag-SR and tiny AgNPs, the signals of S (^{48}S) and Ag (^{107}Ag) were simultaneously recorded by another ICPMS (8800 series, Agilent Technologies, Palo Alto, CA). For both the blank and spiked samples, a peak (t_R = 2.3 min) was detected in the ICPMS profile of ^{48}S, with t_R and peak shape agreeing well with the new ^{107}Ag peak (t_R = 2.3 min). This suggested that the new ^{107}Ag peak at t_R = 2.3 in the spiked

sample should be ascribed to Ag-SR. Unfortunately, the component of Ag-SR could not be further identified based on our available detectors but could be identified off-line by other techniques (e.g., electrospray ionization mass spectrometry) in a future study. To test if tiny AgNPs were present in the transformation process, peak areas of the new ^{107}Ag peak with or without the introduction of H$_2$O$_2$ in the focusing step were compared. No significant difference in peak areas was observed, indicating the absence of tiny AgNPs. Furthermore, we tried to indirectly identify the new ^{107}Ag peak by injecting Ag(I) and the mixture of Ag(I) and cysteine (Cys) into the system, respectively. As shown in Figure S5, the Ag-Cys peak (t_R = 2.5 min) detected in the mixture of Ag(I) and Cys agreed well with the Ag-SR peak (t_R = 2.3 min) in the spiked wastewater sample. These results suggest that the new ^{107}Ag peak detected in the spiked wastewater samples could be solely assigned to Ag-SR, indicating the great potential of the proposed method in separation and identification of various species of Ag(I). In the fractionation step (step II), the spiked AgNPs were eluted at 8.1 min. To test the proposed method in quantifying different species of Ag in complex matrices, the recovery of total Ag (including free Ag(I), Ag-SR, and AgNPs) in spiked solutions was calculated to be within a range from 69.3 to 112%, demonstrating the reliability of the proposed method. Despite the fact that ICPMS equipped with triple quadrupole ICP-MS (ICP-QQQ) is recognized to be able to sensitively and selectively determine S element, no obvious peak was observed in the range of 4−15 min (i.e., the fractionation and characterization of NP step) aside from thiol-complexed Ag(I) together with NOM identified before 4 min in Figure 4, indicating the absence of Ag$_2$S as the sulfidation product of Ag(I) or AgNPs. The relatively short reaction period (i.e., 1 h) in this study likely accounts for the subtle displacement of citrate by S. Thus, long-term incubation (e.g., 120 h)[57] usually needed for the displacement and sulfidation is worthy to study in future.

Environmental Implication. The HF5/MCC-UV/ICPMS system provides an efficient technique to investigate both physical and chemical transformations of AgNPs and Ag(I) at environmentally relevant concentrations. Findings in this study firmly reveal different effects of Ca^{2+} and Na$^+$ on the aggregation of AgNPs at ng/mL in the presence of NOM, facilitating more environmentally meaningful evaluation of the physical transformation of AgNPs under more realistic conditions. The remarkable difference in size of AgNPs generated from photoreduction of Ag(I) at two different concentrations discovered here again highlights the necessity of further studying transformations of AgNPs and Ag(I) at environmentally relevant concentrations in predicting the source and fate of AgNPs in the environment. In addition, the high separation efficiency and anti-interference capability of HF5-based method make it applicable to more complex biological media, such as cellular cultures and body fluids, which is beneficial to estimate potential risks on human and environmental health. Moreover, the high selectivity and multielement detection capability of ICPMS detection make it a prospective method in widely studying the heteroaggregation (e.g., with natural suspended mineral particle) and chemical transformation of AgNPs (e.g., selenylation and sulfidation) and other metal-containing nanoparticles (e.g., the dissolution of CdSe quantum dot) at environmentally relevant concentrations under realistic scenarios.

■ ASSOCIATED CONTENT

S Supporting Information

The Supporting Information is available free of charge on the ACS Publications website at DOI: 10.1021/acs.est.7b03439.

Additional experimental details and results (PDF)

■ AUTHOR INFORMATION

Corresponding Author

*E-mail: jfliu@rcees.ac.cn. Phone: +86-10-62849192.

ORCID Ⓘ

Meseret Amde: 0000-0003-3512-3361

Myeong Hee Moon: 0000-0002-5454-2601

Jing-Fu Liu: 0000-0001-7134-7026

Notes

The authors declare no competing financial interest.

■ ACKNOWLEDGMENTS

■ REFERENCES

(1) Maynard, A. D.; Aitken, R. J.; Butz, T.; Colvin, V.; Donaldson, K.; Oberdorster, G.; Philbert, M. A.; Ryan, J.; Seaton, A.; Stone, V.; Tinkle, S. S.; Tran, L.; Walker, N. J.; Warheit, D. B. Safe Handling of Nanotechnology. *Nature* **2006**, *444* (7117), 267−269.

(2) Yu, S. J.; Yin, Y. G.; Liu, J. F. Silver Nanoparticles in the Environment. *Environ. Sci.: Process Impacts* **2013**, *15* (1), 78−92.

(3) Zhang, C. Q.; Hu, Z. Q.; Deng, B. L. Silver Nanoparticles in Aquatic Environments: Physiochemical Behavior and Antimicrobial Mechanisms. *Water Res.* **2016**, *88*, 403−427.

(4) Fabrega, J.; Fawcett, S. R.; Renshaw, J. C.; Lead, J. R. Silver Nanoparticle Impact on Bacterial Growth: Effect of pH, Concentration, and Organic matter. *Environ. Sci. Technol.* **2009**, *43* (19), 7285−7290.

(5) Lau, B. L. T.; Hockaday, W. C.; Ikuma, K.; Furman, O.; Decho, A. W. A Preliminary Assessment of the Interactions between the Capping Agents of Silver Nanoparticles and Environmental Organics. *Colloids Surf., A* **2013**, *435* (SI), 22−27.

(6) Yang, X. Y.; Jiang, C. J.; Hsu-Kim, H.; Badireddy, A. R.; Dykstra, M.; Wiesner, M.; Hinton, D. E.; Meyer, J. N. Silver Nanoparticle Behavior, Uptake, and Toxicity in *Caenorhabditis Elegans*: Effects of Natural Organic Matter. *Environ. Sci. Technol.* **2014**, *48* (6), 3486−3495.

(7) Levard, C.; Hotze, E. M.; Lowry, G. V.; Brown, G. E. Environmental Transformations of Silver Nanoparticles: Impact on Stability and Toxicity. *Environ. Sci. Technol.* **2012**, *46* (13), 6900−6914.

(8) Dale, A. L.; Lowry, G. V.; Casman, E. A. Stream Dynamics and Chemical Transformations Control the Environmental Fate of Silver and Zinc Oxide Nanoparticles in a Watershed-Scale Model. *Environ. Sci. Technol.* **2015**, *49* (12), 7285−7293.

(9) Yin, Y. G.; Shen, M. H.; Tan, Z. Q.; Yu, S. J.; Liu, J. F.; Jiang, G. B. Particle Coating-Dependent Interaction of Molecular Weight Fractionated Natural Organic Matter: Impacts on the Aggregation of Silver Nanoparticles. *Environ. Sci. Technol.* **2015**, *49* (11), 6581−6589.

(10) Lohrke, J.; Briel, A.; Mäder, K. Characterization of Superparamagnetic Iron Oxide Nanoparticles by Asymmetrical Flow-Field-Flow-Fractionation. *Nanomedicine* **2008**, *3* (4), 437−452.

(11) Chowdhury, I.; Mansukhani, N. D.; Guiney, L. M.; Hersam, M. C.; Bouchard, D. Aggregation and Stability of Reduced Graphene Oxide: Complex Roles of Divalent Cations, pH, and Natural Organic Matter. *Environ. Sci. Technol.* **2015**, *49* (18), 10886−10893.

(12) Loosli, F.; Le Coustumer, P.; Stoll, S. TiO$_2$ Nanoparticles Aggregation and Disaggregation in Presence of Alginate and Suwannee River Humic Acids. pH and Concentration Effects on Nanoparticle Stability. *Water Res.* **2013**, *47* (16), 6052−6063.

(13) Huynh, K. A.; Chen, K. L. Aggregation Kinetics of Citrate and Polyvinylpyrrolidone Coated Silver Nanoparticles in Monovalent and Divalent Electrolyte Solutions. *Environ. Sci. Technol.* **2011**, *45* (13), 5564−5571.

(14) Potera, C. Transformation of Silver Nanoparticles in Sewage Sludge. *Environ. Health. Persp.* **2010**, *118* (12), A526−A527.

(15) Liu, J. Y.; Hurt, R. H. Ion Release Kinetics and Particle Persistence in Aqueous Nano-Silver Colloids. *Environ. Sci. Technol.* **2010**, *44* (6), 2169−2175.

(16) Yin, Y. G.; Liu, J. F.; Jiang, G. B. Sunlight-Induced Reduction of Ionic Ag and Au to Metallic Nanoparticles by Dissolved Organic Matter. *ACS Nano* **2012**, *6* (9), 7910−7919.

(17) Hou, W. C.; Stuart, B.; Howes, R.; Zepp, R. G. Sunlight-Driven Reduction of Silver Ions by Natural Organic Matter: Formation and Transformation of Silver Nanoparticles. *Environ. Sci. Technol.* **2013**, *47* (14), 7713−7721.

(18) Yu, S. J.; Yin, Y. G.; Chao, J. B.; Shen, M. H.; Liu, J. F. Highly Dynamic PVP-Coated Silver Nanoparticles in Aquatic Environments: Chemical and Morphology Change Induced by Oxidation of Ag^0 and Reduction of Ag$^+$. *Environ. Sci. Technol.* **2014**, *48* (1), 403−411.

(19) Braakhuis, H. M.; Cassee, F. R.; Fokkens, P. H. B.; de la Fonteyne, L. J. J.; Oomen, A. G.; Krystek, P.; de Jong, W. H.; van Loveren, H.; Park, M. V. D. Z. Identification of the Appropriate Dose Metric for Pulmonary Inflammation of Silver Nanoparticles in an Inhalation Toxicity Study. *Nanotoxicology* **2016**, *10* (1), 63−73.

(20) Shen, M. H.; Zhou, X. X.; Yang, X. Y.; Chao, J. B.; Liu, R.; Liu, J. F. Exposure Medium: Key in Identifying Free Ag$^+$ as the Exclusive Species of Silver Nanoparticles with Acute Toxicity to *Daphnia magna*. *Sci. Rep.* **2015**, *5*, 9674.

(21) Griffitt, R. J.; Brown-Peterson, N. J.; Savin, D. A.; Manning, C. S.; Boube, I.; Ryan, R.; Brouwer, M. Effects of Chronic Nanoparticulate Silver Exposure to Adult and Juvenile Sheepshead Minnows (*Cyprinodon Variegatus*). *Environ. Toxicol. Chem.* **2012**, *31* (1), 160−167.

(22) Ma, R.; Levard, C. M.; Marinakos, S. M.; Cheng, Y. W.; Liu, J.; Michel, F. M.; Brown, G. E.; Lowry, G. V. Size-Controlled Dissolution of Organic-Coated Silver Nanoparticles. *Environ. Sci. Technol.* **2012**, *46* (2), 752−759.

(23) Chao, J. B.; Liu, J. F.; Yu, S. J.; Feng, Y. D.; Tan, Z. Q.; Liu, R.; Yin, Y. G. Speciation Analysis of Silver Nanoparticles and Silver Ions in Antibacterial Products and Environmental Waters via Cloud Point Extraction-Based Separation. *Anal. Chem.* **2011**, *83* (17), 6875−6882.

(24) Menzel, M.; Fittschen, U. E. A. Total Reflection X-ray Fluorescence Analysis of Airborne Silver Nanoparticles from Fabrics. *Anal. Chem.* **2014**, *86* (6), 3053−3059.

(25) Nakazawa, E.; Ikemoto, T.; Hokura, A.; Terada, Y.; Kunito, T.; Yamamoto, T.; Yamada, T. K.; Rosas, F. C. W.; Fillmann, G.; Tanabe, S.; Nakai, I. Silver Speciation in Liver of Marine Mammals by Synchrotron X-ray Absorption Fine Structure and X-ray Fluorescence Spectroscopies. *J. Environ. Monit.* **2011**, *13* (6), 1678−1686.

(26) Beauchemin, D. Inductively Coupled Plasma Mass Spectrometry. *Anal. Chem.* **2010**, *82* (12), 4786−4810.

(27) Mitrano, D. M.; Ranville, J. F.; Bednar, A.; Kazor, K.; Hering, A. S.; Higgins, C. P. Tracking Dissolution of Silver Nanoparticles at Environmentally Relevant Concentrations in Laboratory, Natural, and Processed Waters Using Single Particle ICP-MS (spICP-MS). *Environ. Sci.: Nano* **2014**, *1* (3), 248−259.

(28) Peters, R.; Herrera-Rivera, Z.; Undas, A.; van der Lee, M.; Marvin, H.; Bouwmeester, H.; Weigel, S. Single Particle ICP-MS Combined with a Data Evaluation Tool as a Routine Technique for the Analysis of Nanoparticles in Complex Matrices. *J. Anal. At. Spectrom.* **2015**, *30* (6), 1274−1285.

(29) Tuoriniemi, J.; Cornelis, G.; Hasellöv, M. Size Discrimination and Detection Capabilities of Single-Particle ICPMS for Environmental Analysis of Silver Nanoparticles. *Anal. Chem.* **2012**, *84* (9), 3965−3972.

(30) Somchue, W.; Siripinyanond, A.; Gale, B. K. Electrical Field-Flow Fractionation for Metal Nanoparticle Characterization. *Anal. Chem.* **2012**, *84* (11), 4993−4998.

(31) Mitrano, D. M.; Barber, A.; Bednar, A.; Westerhoff, P.; Higgins, C. P.; Ranville, J. F. Silver Nanoparticle Characterization Using Single Particle ICP-MS (SP-ICP-MS) and Asymmetrical Flow Field Flow Fractionation ICP-MS (AF4-ICP-MS). *J. Anal. At. Spectrom.* **2012**, *27* (7), 1131−1142.

(32) Huynh, K. A.; Siska, E.; Heithmar, E.; Tadjiki, S.; Pergantis, S. A. Detection and Quantification of Silver Nanoparticles at Environmentally Relevant Concentrations Using Asymmetric Flow Field-Flow Fractionation Online with Single Particle Inductively Coupled Plasma Mass Spectrometry. *Anal. Chem.* **2016**, *88* (9), 4909−4916.

(33) Bolea, E.; Jimenez-Lamana, J.; Laborda, F.; Castillo, J. R. Size Characterization and Quantification of Silver Nanoparticles by Asymmetric Flow Field-Flow Fractionation Coupled With Inductively Coupled Plasma Mass Spectrometry. *Anal. Bioanal. Chem.* **2011**, *401* (9), 2723−2732.

(34) Loeschner, K.; Navratilova, J.; Legros, S.; Wagner, S.; Grombe, R.; Snell, J.; von der Kammer, F.; Larsen, E. H. Optimization and Evaluation of Asymmetric Flow Field-Flow Fractionation of Silver Nanoparticles. *J. Chromatogr. A* **2013**, *1272*, 116−125.

(35) Loeschner, K.; Navratilova, J.; Kobler, C.; Molhave, K.; Wagner, S.; von der Kammer, F.; Larsen, E. H. Detection and Characterization of Silver Nanoparticles in Chicken Meat by Asymmetric Flow Field Flow Fractionation with Detection by Conventional or Single Particle ICP-MS. *Anal. Bioanal. Chem.* **2013**, *405* (25), 8185−8195.

(36) Poda, A. R.; Bednar, A. J.; Kennedy, A. J.; Harmon, A.; Hull, M.; Mitrano, D. M.; Ranville, J. F.; Steevens, J. Characterization of Silver Nanoparticles Using Flow-Field Flow Fractionation Interfaced to Inductively Coupled Plasma Mass Spectrometry. *J. Chromatogr. A* **2011**, *1218* (27), 4219−4225.

(37) Lee, W. C.; Lee, B. T.; Lee, S.; Hwang, Y. S.; Jo, E.; Eom, I. C.; Lee, S. W.; Kim, S. O. Optimisation, Evaluation and Application of Asymmetrical Flow Field-Flow Fractionation with Single Particle Inductively Coupled Plasma Mass Spectrometry (SP-ICP-MS) to Characterise Silver Nanoparticles in Environmental Media. *Microchem. J.* **2016**, *129*, 219−230.

(38) Zattoni, A.; Casolari, S.; Rambaldi, D. C.; Reschiglian, P. Hollow-Fiber Flow Field-Flow Fractionation. *Curr. Anal. Chem.* **2007**, *3* (4), 310−323.

(39) Reschiglian, P.; Zattoni, A.; Roda, B.; Cinque, L.; Parisi, D.; Roda, A.; Dal Piaz, F.; Moon, M. H.; Min, B. R. On-Line Hollow-Fiber Flow Field-Flow Fractionation-Electrospray Ionization/Time-of-Flight Mass Spectrometry of Intact Proteins. *Anal. Chem.* **2005**, *77* (1), 47−56.

(40) Marassi, V.; Casolari, S.; Roda, B.; Zattoni, A.; Reschiglian, P.; Panzavolta, S.; Tofail, S. A. M.; Ortelli, S.; Delpivo, C.; Blosi, M.; Costa, A. L. Hollow-Fiber Flow Field-Flow Fractionation and Multi-Angle Light Scattering Investigation of the Size, Shape and Metal-Release of Silver Nanoparticles in Aqueous Medium for Nano-Risk Assessment. *J. Pharm. Biomed. Anal.* **2015**, *106* (SI), 92−99.

(41) Tan, Z. Q.; Liu, J. F.; Guo, X. R.; Yin, Y. G.; Byeon, S. K.; Moon, M. H.; Jiang, G. B. Toward Full Spectrum Speciation of Silver Nanoparticles and Ionic Silver by On-Line Coupling of Hollow Fiber Flow Field-Flow Fractionation and Minicolumn Concentration with Multiple Detectors. *Anal. Chem.* **2015**, *87* (16), 8441−8447.

(42) Kim, H. J.; Oh, S.; Moon, M. H. Hollow-Fiber Flow/Hyperlayer Field-Flow Fractionation for the Size Characterization of Airborne Particle Fractions Obtained by SPLITT Fractionation. *J. Sep. Sci.* **2006**, *29* (3), 423−428.

(43) Gigault, J.; Hackley, V. A. Observation of Size-Independent Effects in Nanoparticle Retention Behavior during Asymmetric-Flow Field-Flow Fractionation. *Anal. Bioanal. Chem.* **2013**, *405* (19), 6251−6258.

(44) Heroult, J.; Nischwitz, V.; Bartczak, D.; Goenaga-Infante, H. The Potential of Asymmetric Flow Field-Flow Fractionation Hyphenated to Multiple Detectors for the Quantification and Size Estimation of Silica Nanoparticles in a Food Matrix. *Anal. Bioanal. Chem.* **2014**, *406* (16), 3919−3927.

(45) Li, X.; Lenhart, J. J.; Walker, H. W. Aggregation Kinetics and Dissolution of Coated Silver Nanoparticles. *Langmuir* **2012**, *28* (2), 1095−1104.

(46) Maurice, P. A.; Pullin, M. J.; Cabaniss, S. E.; Zhou, Q. H.; Namjesnik-Dejanovic, K.; Aiken, G. R. A Comparison of Surface Water Natural Organic Matter in Raw Filtered Water Samples, XAD, and Reverse Osmosis Isolates. *Water Res.* **2002**, *36* (9), 2357−2371.

(47) Lowry, G. V.; Gregory, K. B.; Apte, S. C.; Lead, J. R. Transformations of Nanomaterials in the Environment. *Environ. Sci. Technol.* **2012**, *46* (13), 6893−6899.

(48) Yuan, W.; Zydney, A. L. Effects of Solution Environment on Humic Acid Fouling during Microfiltration. *Desalination* **1999**, *122* (1), 63−76.

(49) Akaighe, N.; Depner, S. W.; Banerjee, S.; Sharma, V. K.; Sohn, M. The effects of Monovalent and Divalent Cations on the Stability of Silver Nanoparticles Formed from Direct Reduction of Silver Ions by Suwannee River Humic Acid/Natural Organic Matter. *Sci. Total Environ.* **2012**, *441*, 277−289.

(50) Zou, X. Y.; Li, P. H.; Lou, J.; Fu, X. Y.; Zhang, H. W. Stability of Single Dispersed Silver Nanoparticles in Natural and Synthetic Freshwaters: Effects of Dissolved Oxygen. *Environ. Pollut.* **2017**, *230*, 674−682.

(51) Parker, K. M.; Pignatello, J. J.; Mitch, W. A. Influence of Ionic Strength on Triplet-State Natural Organic Matter Loss by Energy Transfer and Electron Transfer Pathways. *Environ. Sci. Technol.* **2013**, *47* (19), 10987−10994.

(52) Jones, K. L.; O'Melia, C. R. Protein and Humic Acid Adsorption onto Hydrophilic Membrane Surfaces: Effects of pH and Ionic Strength. *J. Membr. Sci.* **2000**, *165* (1), 31−46.

(53) Assemi, S.; Tadjiki, S.; Donose, B. C.; Nguyen, A. V.; Miller, J. D. Aggregation of Fullerol $C_{60}(OH)_{24}$ Nanoparticles as Revealed Using Flow Field-Flow Fractionation and Atomic Force Microscopy. *Langmuir* **2010**, *26* (20), 16063−16070.

(54) Kim, S. T.; Lee, Y. J.; Hwang, Y. S.; Lee, S. Study on Aggregation Behavior of Cytochrome C-Conjugated Silver Nanoparticles Using Asymmetrical Flow Field-Flow Fractionation. *Talanta* **2015**, *132*, 939−944.

(55) Yin, Y. G.; Shen, M. H.; Zhou, X. X.; Yu, S. J.; Chao, J. B.; Liu, J. F.; Jiang, G. B. Photoreduction and Stabilization Capability of Molecular Weight Fractionated Natural Organic Matter in Transformation of Silver Ion to Metallic Nanoparticle. *Environ. Sci. Technol.* **2014**, *48* (16), 9366−9373.

(56) Mueller, N. C.; Nowack, B. Exposure Modeling of Engineered Nanoparticles in the Environment. *Environ. Sci. Technol.* **2008**, *42* (12), 4447−4453.

(57) Azodi, M.; Sultan, Y.; Ghoshal, S. Dissolution Behavior of Silver Nanoparticles and Formation of Secondary Silver Nanoparticles in Municipal Wastewater by Single Particle ICP-MS. *Environ. Sci. Technol.* **2016**, *50* (24), 13318−13327.